IUPAC Technical Report

Clive Bucknall*, Volker Altstädt, Dietmar Auhl, Paul Buckley, Dirk Dijkstra, Andrzej Galeski, Christoph Gögelein, Ulrich A. Handge, Jiasong He, Chen-Yang Liu, Goerg Michler, Ewa Piorkowska, Miroslav Slouf, Iakovos Vittorias and Jun Jie Wu

Structure, processing and performance of ultra-high molecular weight polyethylene (IUPAC Technical Report). Part 2: crystallinity and supra molecular structure

Abstract: Test methods including OM, SEM, TEM, DSC, SAXS, WAXS, and IR were used to characterise supra-molecular structure in three batches of polyethylene (PE), which had weight-average relative molar masses $\overline{M}_w$ of approximately 0.6×10^6, 5×10^6, and 9×10^6. They were applied to compression mouldings made by the polymer manufacturer. Electron microscopy showed that powders formed in the polymerization reactor consisted of irregularly shaped grains between 50 and 250 µm in diameter. Higher magnification revealed that each grain was an aggregate, composed of particles between 0.4 and 0.8 µm in diameter, which were connected by long, thin fibrils. In compression mouldings, lamellar thicknesses ranged from 7 to 23 nm. Crystallinity varied between 70 and 75 % in reactor powder, but was lower in compression mouldings. Melting peak temperatures ranged from 138 to 145 °C, depending on processing history. DMTA showed that the glass transition temperature θ_g was –120 °C for all three grades of polyethylene. IR spectroscopy found negligibly small levels of oxidation and thermal degradation in mouldings. Optical microscopy revealed the presence of visible fusion defects at grain boundaries. It is concluded that relatively weak defects can be characterized using optical microscopy, but there is a need for improved methods that can detect less obvious fusion defects.

*Corresponding author: Clive Bucknall, School of Aerospace, Transport & Manufacturing B 61, Cranfield University, Bedford, MK43 0AL, UK, e-mail: clivebucknall@aol.com

Volker Altstädt: Department of Polymer Engineering, Universität Bayreuth, Bayreuth, Germany

Dietmar Auhl: Fakultät III – Werkstoffwissenschaft Technische Universität Berlin, D-10623, Berlin, Germany

Paul Buckley: Department of Engineering Science, University of Oxford, OX1 3PJ, Oxford, UK

Dirk Dijkstra: Covestro Deutschland AG, Leverkusen, Germany

Andrzej Galeski and Ewa Piorkowska: Centre for Molecular and Macromolecular Sciences, Polish Academy of Sciences, Lodz, Poland

Christoph Gögelein: Arlanxeo Deutschland GmbH, Dormagen, Germany

Ulrich A. Handge: Institute of Polymer Research, Helmholtz-Zentrum Geesthacht, Max-Planck-Strasse 1, 21502, Geesthacht, Germany

Jiasong He and Chen-Yang Liu: Chinese Academy of Sciences, Laboratory of Polymer Science and Materials, Beijing, 100190, China

Goerg Michler: Martin-Luther-Universität Halle-Wittenberg, Germany

Miroslav Slouf: Institute of Macromolecular Chemistry CAS, Prague, Czech Republic

Iakovos Vittorias: Omya International AG, Baslerstrasse 42, CH-4665, Oftringen, Switzerland

Jun Jie Wu: Department of Engineering, Durham University, Stockton Road, Durham, DH1 3LE, UK

CONTENTS

1 Introduction

This is the second of four reports from IUPAC Sub-Committee 4.2.1: Structure and Properties of Commercial Polymers, which set up a Task Group to evaluate the effectiveness of available test methods for quality control and quality assurance of products made from ultra-high molecular weight polyethylene (UHMWPE), which is used as a bearing material in artificial joints.

The term 'ultra-high molecular weight' is applied to grades of polyethylene (PE) with weight average relative molar masses $\overline{M}_\mathrm{w}$ greater than 10^6. The authors note that 'molecular weight', which features in the title of this report, is the historical name for relative molar mass. Except where numerical values are given, it will therefore be used throughout this report, to be consistent with the widely accepted name for UHMWPE.

The reasons for initiating a large-scale collaborative study of these materials are explained in Part 1 of this series [1]. As the most demanding applications of UHMWPE are in total knee- and hip-joint replacements [2], very high standards of quality control (QC) and quality assurance (QA) should be applied during their manufacture. However, limited solubility, high melt viscosity, and long relaxation times, which are characteristic of this range of polymers, make this goal difficult to achieve. Part 1 considers the limitations of available methods for measuring the weight-average molecular weight of a UHMWPE sample, and notes that it is currently impossible to determine distributions of molecular weight, because solutions made from commercial grades of UHMWPE inevitably contain some entangled gels, which clog permeation columns. The present report is concerned with the structures found in compression mouldings, especially their crystallinity, crystal structure, and grain-boundary defects. Part 3 examines the effects of molecular weight, crystallinity, fusion defects, and other structural features on the basic mechanical properties of moulded UHMWPE, and Part 4 examines the extraordinary effects of fusion defects on fatigue crack propagation in compression mouldings supplied by the polymer manufacturer.

We note that a desire to improve the processability, structure, and properties of UHMWPE has led to the development of single-site catalytic systems for the synthesis of these polymers [3]. This might make it possible in the future to measure molecular weight distributions in commercial grades of UHMWPE and minimise the effects of fusion defects on the formation of polyethylene wear particles in joint prostheses. As our work is restricted to commercial polymers, these developments lie beyond the scope of the present report.

2 Experiments and results

2.1 Materials

In support of this project, a leading manufacturer provided three large batches of UHMWPE powder, which had nominal weight-average relative molar masses, $\overline{M}_{\mathrm{w}}$, of approximately 0.6×10^6, 5×10^6, and 9×10^6, respectively. Accordingly, they were given the code names PE06, PE5, and PE9. Unless otherwise stated, all results presented in this report were obtained from tests on compression mouldings made by the polymer manufacturer under standardized processing conditions.

2.2 Morphology of powder particles – scanning electron microscopy

The first step in characterizing structure in PE06, PE5, and PE9 was to determine the dimensions and morphology of powder particles obtained from the polymerization reactor. Scanning electron microscopy undertaken by Michler (code ML)[1] showed very little difference between the three grades at this stage. Typical morphology is illustrated in Fig. 1. At a low magnification, PE9 powder is seen to consist of irregularly shaped grains with diameters between 50 and 250 μm. However, higher magnification revealed that each grain is an aggregate of much smaller, roughly spherical particles, with diameters between 0.4 and 0.8 μm. Some of these small particles had fused together. Others were connected by long, straight fibrils between 50 and 75 nm in diameter. Similar features have been reported in previous publications, most notably in an encyclopedia article by Kurtz [2]. Their formation can be attributed to continuous swelling of the spherical microparticles as the polymer chains increased in length. That swelling eventually led to the formation of macroparticles when the microparticles came into contact, and at some stage chain entanglement probably occurred at the contact points. During subsequent polymerization, both the microparticles and the macroparticles continued to expand to accommodate freshly-formed polymer. Also, in some less densely populated regions, the contacting microparticles were pulled apart as a result of this expansion, thereby forming the extended fibrils seen at high magnification in Fig. 1 [4, 5].

2.3 Lamellar morphology – TEM and SEM

Michler (code ML) used transmission electron microscopy (TEM) to characterize lamellar morphology in PE06, PE5, and PE9. Samples cut from compression mouldings were embedded in epoxy resin, repeatedly exposed to RuO_4 vapour, and sectioned using a Leica Ultracut UCT ultramicrotome fitted with a Diatome diamond knife, to produce sections about 80 nm thick. A typical section is shown in Fig. 2. Each section revealed linear features, which were previously identified as lamellae seen edge-on [6]. The lamellae have a broad distribution of thicknesses, ranging approximately from 7 to 28 nm, with a peak at (16 ± 3) nm.

    A group led by Slouf used scanning electron microscopy (SEM) to study lamellae in PE06, PE5, and PE9. Specimen blocks were cut from the centres of compression mouldings. Smooth surfaces were then prepared by microtoming at room temperature and etched with a permanganic mixture, as described in an earlier article [7]. The etched surfaces were covered with a 4 nm thick platinum layer using a Balzers SCD 050 vacuum sputter coater and observed using a secondary electron detector at an accelerating applied potential of 15 kV. The results are presented in Fig. 3, where projecting crystalline lamellae are seen as bright features against a dark background.

---

1 Each laboratory participating in this project is identified by a two-letter code – see Part 1, Table 1.
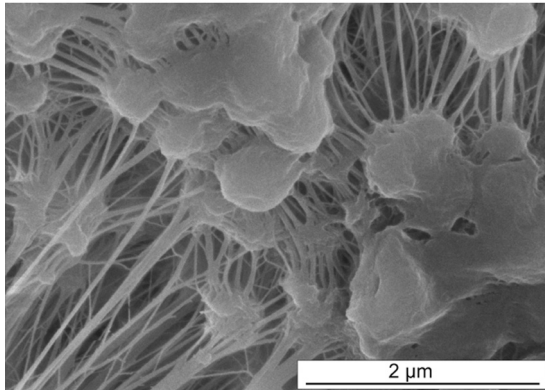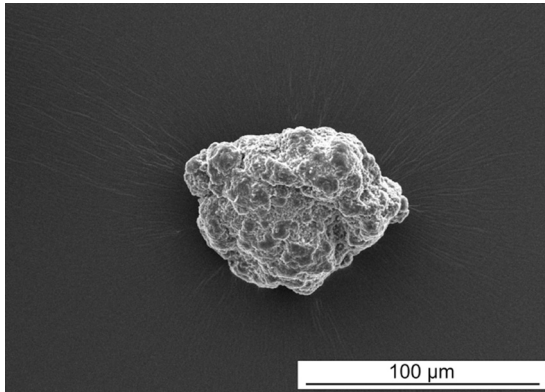
Fig. 1: Reactor powder particles of PE9 viewed at two magnifications – transmission electron micrographs provided by Michler (laboratory code ML).
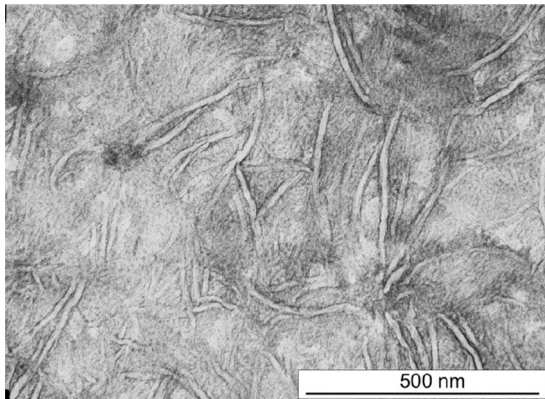

Fig. 2: Transmission electron micrograph of a section through embedded PE9 particles at a high magnification. Michler (ML).

2.4 Crystallinity and signs of degradation – infrared spectroscopy

Slouf (CZ) used infra-red spectroscopy to measure crystallinity and check for signs of degradation in moulded plaques. This technique is helpful in identifying chemical changes in UHMWPE bearing surfaces, especially in total joint replacements [8]. All three grades of PE feature notable peaks in the IR spectrum at 1303 and 1897 cm^{-1}, which are characteristic of the amorphous and crystalline components, respectively. Crystallinity was calculated from the areas of these two peaks. The values obtained corresponded to 70.6 % by weight in PE06, 57.8 % in PE5, and 55.8 % in PE9, with combined standard uncertainty, u_c, of ±2 % of the measured value.
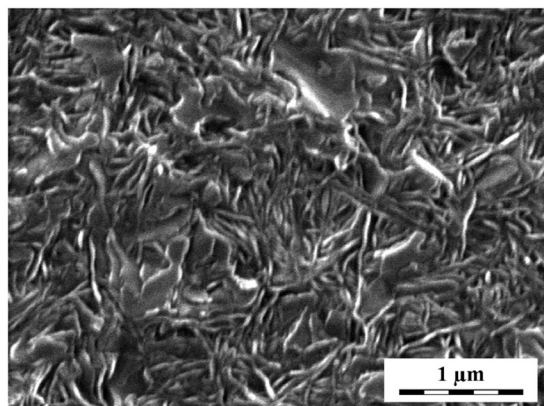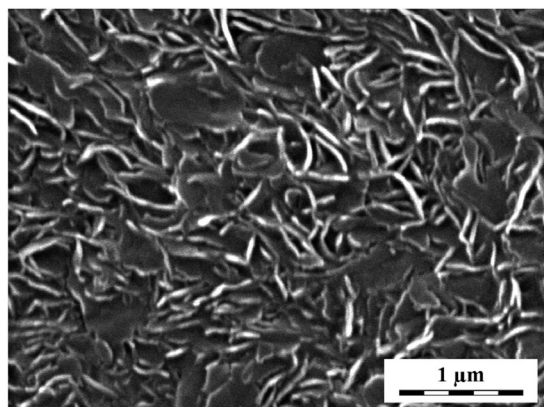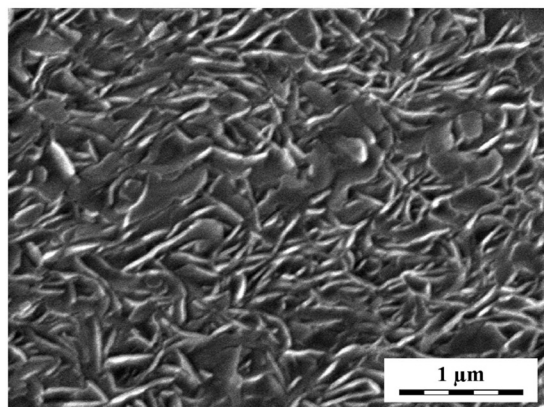
Fig. 3: Scanning electron micrographs showing lamellar structure in PE06, PE5, and PE9, revealed by microtoming followed by etching with permanganic acid. Slouf (code CZ).

Published studies have shown that degradation of PE samples results in peaks in the infra-red spectrum that indicate oxidation (>C=O at 1715 cm^{-1}) and crosslinking (trans>C=C< at 960 cm^{-1}). In the present study, measurements were made at three locations in a single specimen of each polymer. Both oxidation and trans-vinylene crosslinking peaks were negligibly small, with an integral intensity close to zero in all three grades of PE.

2.5 Crystallinity, crystallization and melting – SAXS, WAXS, DSC

Galeski (PA) used small-angle X-ray scattering (SAXS) to study lamellar thicknesses in compression moulded discs that were 25 mm thick and 136 mm in diameter. Two slices, 0.6 mm thick, were machined from a single

disc of each material, one on a plane containing the central compression axis and the other on a plane parallel to the tangential surface of the disc. Lamellar structure was characterized using two-dimensional small angle X-ray scattering (2-D SAXS). A Kissing-type camera was placed at a distance of 1.2 m from the sample and coupled to a low-divergence CuK$_\alpha$ X-ray micro-source operating at 50 kV and 1 mA (GeniX Cu-LD from Xenics, France). The sealed-tube micro-source was integrated with multilayer collimation optics to produce a highly collimated beam with a divergence of 0.8×0.8 mrad^2. The collimation optics were combined with two additional hybrid scatter-free slit systems to produce a beam with a square cross-section. The two slit assemblies were placed 1.2 m apart. Scattering produced by the sample was recorded by a Pilatus 100 K solid-state detector with a resolution of 172×172 μm^2 (Dectris, Switzerland). For unoriented samples, the long period (P_L) was determined by applying Bragg's law to 1D sections through 2-D scattering patterns. Background and Lorentz corrections were applied.

Figure 4 compares SAXS patterns from PE06, PE5, and PE9. They show that the lamellae in PE5 and PE9 are distributed preferentially on planes perpendicular to the compression axis of the disc, but there is no orientation in PE06, where the directions of lamellar axes are randomly distributed. Fig. 5 shows the relationship for all three grades of polyethylene between the scattering vector q and Iq^2, where I is the scattering intensity at angle θ, q is given by:

$$q = \frac{4\pi \sin\theta}{\lambda} \tag{1}$$

and λ is the X-ray wavelength. Long period (P_L) values determined from peaks in the SAXS profiles according to Bragg's Law were 34.5, 41.5, and 44.5 nm for PE06, PE5, and PE9 respectively. Lamellar thicknesses, calculated from density correlation functions, were 9.5, 11.8, and 11.3 nm for PE06, PE5, and PE9 respectively, with a u_c of $\pm 3\%$. All three grades of UHMWPE have similar scattering profiles, except for a shift along the q axis due to reduced lamellar thickness in PE06, which can also be seen in Fig. 2. For this polymer, there is no sign of an extended tail at higher scattering angles, which would indicate the presence of thinner, more easily deformed lamellae.

Slouf (CZ) carried out small-angle and wide-angle X-ray scattering (SAXS and WAXS) tests on sections cut in three mutually perpendicular directions from compression moulded PE06, PE5, and PE9 discs. Cutting was performed under intense cooling in order to minimize changes in supramolecular structure. The first pair of samples (XZ and YZ) were cut parallel to the compression direction (Z axis). The second pair of samples, designated XYi and XYe, were cut on planes lying normal to the compression direction, where letters i and e denote interior and edge locations on the disc, respectively. This procedure made it possible to study the effects of orientation and sub-surface depth on supra-molecular structure. A Freiberger Präzisionsmechanik HZG/4A powder diffractometer was used to obtain a complete set of one-dimensional WAXS (1D-WAXS) patterns for PE06, PE5, and PE9. Samples XZ, YZ, XYi, and XYe were examined in two orientations, parallel (‖) and perpendicular (⊥) to the long edges of the machined sections. Two-dimensional WAXS (2D-WAXS) and SAXS (2D-SAXS) diffraction patterns were recorded using a pinhole camera (Molecular Metrology SWAXS System) attached to a micro-focused X-ray beam generator (Osmic MicroMax 002) operating at 45 kV and 0.66 mA (30 W). Crystallinity, χ_c, was calculated from the ratio of I_{cr}, the integral intensity of diffraction from the crystalline phase, to I_{tot}, the total diffraction intensity. The 2D-SAXS patterns were converted to one-dimensional (1D) curves, with the Lorentz correction applied. Peak positions (q_m) were used to obtain long periods (P_L) according to Bragg's law.

The results are shown in Table 1. Apart from two anomalously high readings in the 1D⊥ column, the data are consistent with the other data recorded in this report. Crystallinity was substantially higher in PE06 than in the two UHMWPE grades and long periods increased with molecular weight.

Slouf also used differential scanning calorimetry to measure crystallinity in compression moulded discs. Tests were carried out, under nitrogen at a heating rate of 10 K min^{-1}, using a Perkin-Elmer Pyris1 DSC. For each material, measurements were made on three separate samples, each taken from the centre of a single moulded disc. Average crystallinity values obtained were 56.4 % in PE06, 35.8 % in PE5, and 37.8 % in PE9, with uncertainty $u_c = \pm 3\%$.
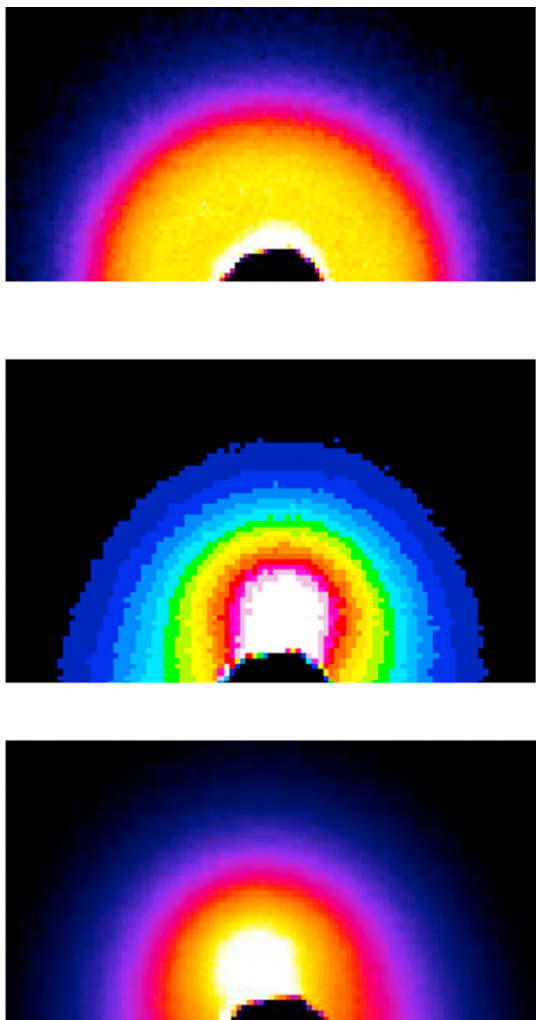
Fig. 4: SAXS patterns for PE06 (top), PE5 (middle), and PE9 (bottom). Galeski (code PA).
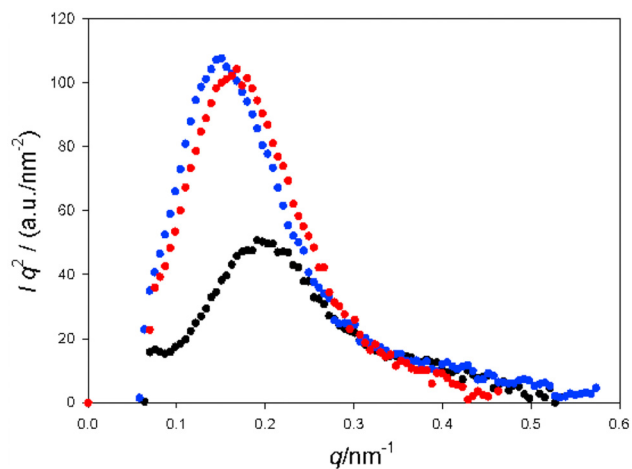
Fig. 5: SAXS profiles for compression moulded PE06 (black), PE5 (red), and PE9 (blue). Galeski (PA).

Handge (code HG) and Piorkowska (code PA) measured crystallinity using TA Instruments differential scanning calorimeters, models Q1000 and Q20. Samples between 4 and 6 mg were cut from the centres of compression-moulded plaques and heated under nitrogen at 10 K min^{-1}. They were cooled to room temperature

Table 1: Crystallinity, χ_c, with combined standard uncertainty $u_c = \pm 2.5$ %, and long period P_L, with $u_c = \pm 3$ %. Values for compression-moulded PE06, PE5 and PE9, obtained using WAXS and SAXS. Data of Slouf (CZ).

| Polymer	Section	χ_c/%			P_L/nm	
		1D ‖	**1D ⊥**	**2D**	**1st peak**	**2nd peak**
PE06	XYi	59	59	61	31.4	16.1
	XYe	59	61	60	31.4	17.4
	XZ	61	60	60	31.4	18.0
	YZ	59	63	62	31.4	17.4
PE5	XYi	43	45	42	39.2	19.0
	XYe	44	55	48	39.2	18.5
	XZ	43	44	44	39.2	19.0
	YZ	43	49	45	39.2	19.0
PE9	XYi	40	40	43	44.9	20.9
	XYe	40	55	46	44.9	19.6
	XZ	43	41	43	44.9	20.9
	YZ	41	49	46	44.9	19.6

and then heated again at 10 K min^{-1}. Percentage crystallinity was calculated assuming a specific enthalpy of fusion $\Delta_{fus}H^0$ of 293 kJ kg^{-1} [9]. The same value of $\Delta_{fus}H^0$ was used for all calculations of crystallinity in polyethylene presented in this report.

The data shown in Table 2 are averages from two separate samples of each polymer. They demonstrate that crystallinity was much higher in PE06 than in PE5 and PE9 and that the same relationship was maintained through both heating stages, although levels of crystallinity increased after the first heating stage. These effects are in line with expectations. Hoffman and Miller have explained the reduced crystallinity of UHMWPE as the result of many macromolecular chains being involved in two or more adjacent lamellae, or at two widely-separated locations in a single lamella, so that chain segments between these anchor points have less freedom to participate in crystallization than those with unrestricted chain ends [10].

At any given temperature, the relaxation times in the non-crystalline phase are shorter in PE06 than they are in the two UHMWPE grades. Consequently, as the polymer cools in the mould, PE06 is able to come closest to the levels of crystallinity that are found, for example, in extrusion grades of linear polyethylene.

Piorkowska (PA) also used DSC to measure the melting point temperatures, θ_m, of powders. Her results are presented in Table 3. They show a substantial decrease in θ_m between nascent powder and samples that had been melted, cooled, and reheated. It should be noted that the powders have higher crystallinities than the compression moulded samples.

2.6 High pressure crystallization

Figure 6 is a schematic phase diagram for UHMWPE. The triple point was found at about 360 MPa and 215 to 220 °C. We note that Hikosaka et al. concluded that the triple point pressure and temperature were higher by at least 50 MPa and 20 degrees, respectively, based on experiments on a high-density polyethylene with a relatively low molecular weight [11].

Table 2: Effects of heating and cooling on percentage crystallinity, χ_c, of compression moulded HMWPE, with combined standard uncertainty $u_c = \pm 2.5$ %. Handge (HG), Piorkowska (PA).

Polymer			χ_c/%
	1st heating	**1st cooling**	**2nd heating**
PE06	63.6	65.4	65.3
PE5	52.4	55.0	55.0
PE9	52.3	54.1	53.9

Table 3: Melting point temperatures, θ_m (with combined standard uncertainty u_c ±0.5 °C) and percentage crystallinity (with $u_c = \pm2.5$ %) of nascent powder samples. DSC, heating rate of 10 K min⁻¹. Data of Piorkowska (PA).

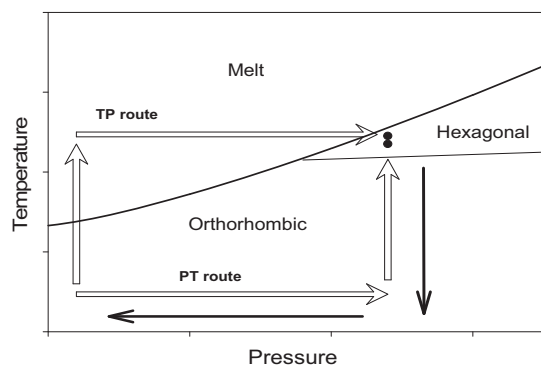| DSC heating			θ_m/ °C
	PE06	PE5	PE9
1ˢᵗ heating	138.0	141.8	142.5
2ⁿᵈ heating	134.4	132.5	132.4
χ_c/%			
1ˢᵗ heating	76.5	72.4	71.3

Fig. 6: Schematic phase diagram for polyethylene, showing TP and PT routes to the region in which hexagonal crystals are stable. On the TP route, the temperature is raised from 23 to 235 °C or 245 °C at atmospheric pressure, and the pressure is then raised to 480 MPa. On the PT route, the pressure is raised to 480 MPa, and the samples are then heated to 235 or 245 °C. Black arrows mark return paths for both routes [2, 11].

As indicated by the arrows and black points, the region in which hexagonal crystals are stable can be reached by raising the temperature to 235 or 245 °C and applying pressure to the melt (TP route) or by applying a pressure greater than 360 MPa to the sample and heating it to 235 or 245 °C to induce a solid state phase transformation (PT route). These transformations are particularly interesting, because experiments on standard grades of linear polyethylene show that entanglement densities decrease substantially under these conditions and thick pseudo-hexagonal crystals are formed [12–14]. In the hexagonal phase, lamellae also grow thicker than they do in the orthorhombic phase, so that X-ray reflections are difficult (or in some cases impossible) to detect. Furthermore, the structural changes induced in the hexagonal phase are not reversed when the sample is cooled to room temperature [15, 16].

In the present project, a group led by Piorkowska (PA) studied the effects of crystallization under high pressure on melting, crystallization, and phase transformation in PE06, PE5, and PE9. Following procedures used in earlier studies on medium molecular weight grades of linear polyethylene, they used an Instron tensometer fitted with a specially-designed high-pressure cell to compress samples of reactor powder between tightly-fitting 9.5 mm diameter plungers. A full description of the equipment used for this work is given by Masirek and co-workers [16]. Pressures and temperatures were controlled to an accuracy of ±0.5 MPa and ±1 K and applied sequentially, as illustrated in Fig. 6. On the TP route, a pressure of 1.5 MPa was first applied for 5 min to compact the powder slightly. The temperature was then raised to 235 or 245 °C, and the sample was held for 5 min before the pressure was increased to 480 MPa. When the PT route was followed, the pressure was first increased to 480 MPa, and the temperature was then raised to 235 or 245 °C. After annealing for 1 or 2 h, all samples were cooled to room temperature under full pressure, thereby inducing a solid-state transformation from pseudo-hexagonal to orthorhombic crystals.

The melting temperatures, θ_m, and enthalpies of fusion, $\Delta_{fus}H^0$ of both nascent powder and annealed samples were measured using a TA Instruments DSC 2920 calorimeter. Samples were heated to 200 °C at 10 K min⁻¹, cooled to room temperature, and then heated again to 200 °C.

The results of these tests are compared in Tables 4 and 5. They show that both θ_m and $\Delta_{fus}H^0$ increase during annealing at elevated pressure and temperature, the extent of the increase depending on the molecular weight of the polymer, the duration of annealing, and the sequence in which pressure and temperature are

raised. In the case of PE06, χ_c increased from 76 % in the powder to about 90 % in annealed samples. High pressure annealing led to thickening of existing crystals (PT route) or to the formation of thick crystals from the melt (TP route). It can also reduce the number of chain folds and hence the free energy of basal surfaces of crystals.

The observed increase in melting temperatures is directly related to an increase in lamellar thickness L^*, in accordance with the Gibbs-Thomson equation:

$$L^* = \frac{2G_e T_m^0}{\Delta_{fus}H^0\left(T_m^0 - T_m\right)} \tag{2}$$

where G_e is the lamellar basal surface free energy, $\Delta_{fus}H^0$ is the heat of fusion, and T_m^0 is the extrapolated equilibrium melting point. For PE, G_e is 9 μJ cm^{-2} and T_m^0 is 418.2 K [16]. In the limit, the chains are fully extended and there are no lamellae left. It is possible to reach this state in standard grades of HDPE, in which $\overline{M}_w$ is less than 10^5, but not in UHMWPE, because relaxation rates are too low at all temperatures that do not cause degradation.

It should be noted that θ_m values for UHMWPE samples crystallized under high pressures exceeded θ_m^0 in some cases. This indicates that the crystals were not only very thick but were also severely constrained. It is reasonable to conclude that extremely long crystallization times would be required to reach a state in which the chains are fully extended, and that a significant amount of thermal degradation would take place during this period. It is interesting to note that the PE5 and PE9 samples had higher melting points than PE06 samples that were crystallized under the same conditions. The crystallinity reached at high pressures was also higher in the PE06 samples than in the PE5 and PE9 samples, as in samples crystallized under atmospheric pressure.

Table 4: Effects of high-pressure annealing conditions (time, temperature, processing route) on melting temperature θ_m ($u_c = \pm0.5$ °C) of HMWPE and UHMWPE. DSC tests, heating rate 10 K min^{-1}. Data of Piorkowska (PA).

Treatment			θ_m/°C
	PE06	**PE5**	**PE9**
1 h 235 TP	143.9	146.1	146.6
1 h 235 PT	144.0	147.4	146.9
1 h 245 PT	143.9	144.6	147.0
2 h 235 TP	146.8	149.6	147.3
2 h 245 TP	145.2	146.8	147.8
2 h 235 PT	143.5	147.4	147.0
2 h 245 PT	142.9	146.0	146.0

Table 5: Effects of high pressure annealing on percentage crystallinity χ_c ($u_c = \pm2.5$ %). Based on DSC data of Piorkowska (PA).

Treatment			χ_c/%
	PE06	**PE5**	**PE9**
1 h 235 TP	89.1	75.8	73.4
1 h 235 PT	88.7	78.8	84.6
1 h 245 PT	88.7	75.8	83.3
2 h 235 TP	87.4	79.2	73.7
2 h 245 TP	80.5	68.6	63.5
2 h 235 PT	88.4	78.5	82.3
2 h 245 PT	89.8	76.5	78.8

2.7 Fusion defects

To study the effects of processing conditions on the integrity of UHMWPE mouldings, Buckley (code OU) compression moulded three sets of plaques, at 150, 165, and 180 °C, respectively. Those dwell temperatures were selected on the basis of preliminary trials, which showed that mouldings made below 150 °C were too brittle to be machined and that processing above 180 °C produced no obvious improvements in strength. Dwell times at maximum temperature and full pressure were limited to 15 min. Applied pressure was kept relatively low during initial heating, then raised to 9 MPa when the mould reached 145 °C. After consolidation at the selected dwell temperature, the 3 mm thick mouldings were cooled rapidly under full pressure. Measurements based on Archimedes' principle then gave densities of 954, 935, and 932 kg m^{-3} for PE06, PE5, and PE9, respectively.

Specimens cut from these mouldings were subjected to two types of tensile test at room temperature. In standard tests, specimens were stretched at constant strain rate, either to failure or to the limit of the extensometer, which in these experiments was reached when the specimens reached 600 % extension. In cyclic tests, specimens were repeatedly taken to a fixed strain, ε_{max}, unloaded to zero stress, and returned to ε_{max}. For the first four cycles, ε_{max} was set at 40 %. During the fifth cycle, ε_{max} was raised to 60 %. The specimen was subjected to a further four cycles with ε_{max} at 60 %. For the final five cycles, ε_{max} was increased to 80 %. The stress-strain behaviour observed during these tests is discussed in Part 3.

Optical microscopy (OM) and environmental scanning electron microscopy (ESEM) were used to study structure in the compression moulded specimens before and after tensile testing. Previous work showed that the PTFE spray used as a release agent in this program leaves a fine coating of PTFE particles on the moulded surfaces. Most of these were removed by washing with an acetone solution; subsequent inspection using ESEM found only a small scattering of PTFE particles. Sections approximately 50 μm thick were prepared using a sledge microtome and sandwiched between cover slips in a fluid with a refractive index matching the sample.

In optical microscopy, sections from untested PE06 showed no visible evidence of grain-boundary fusion defects. After load cycling, the tensile bars became significantly whiter, but it was not possible to see individual voids, which suggests that they were all below the limit of resolution for light microscopy (about 0.2 μm). Controlled cavitation of this type usually has the effect of enhancing the fracture resistance of the polymer. It reduces constraints close to the notch tip while leaving the load-bearing network of highly-stressed chains essentially intact [17]. The same toughening mechanism is responsible for the fracture resistance of all commercial grades of rubber-modified thermoplastics, including ABS, high-impact polystyrene, toughened PVC, and super-tough polyamides [18, 19]. From that perspective, polyethylene can be regarded as a rubber-toughened thermoplastic, in which PE chains form both the rigid, continuous crystalline phase and the particulate elastomeric amorphous phase in which cavitation is initiated.

Figure 7 shows a pattern of discrete domains in an untested PE9 specimen, with domain sizes corresponding approximately to the dimensions of reactor powder particles (50 to 250 μm). Similar patterns are seen in Fig. 8, where the section was taken from a cyclically loaded PE5 specimen. The faint parallel lines running horizontally across the micrograph are due to small irregularities in the cutting edge of the microtome blade. It is possible that forces imposed by the blade were responsible for exposing weak inter-particle boundaries in both specimens. The effects of cyclic loading are not apparent in Fig. 8.

Evidence for inter-particle shear was obtained by concentrating on areas where the microtome blade cut through the outer surface of a tensile bar. Fig. 9 compares two sections viewed under polarized light. Before testing, the surfaces of test specimens were flat and featureless. After cyclic loading, they were roughened to a depth of about 15 μm, owing to unhindered shear at inter-particle boundaries adjacent to the surface.

An alternative method for observing fusion defects, dark field imaging, is illustrated in Fig. 10. Dark field imaging is a special technique for observing discontinuities in translucent specimens using light microscopy. The images are formed only by scattered light, so that tiny holes and intergranular impurities produce bright spots, while larger holes and featureless solid regions appear black in the micrographs. Other types of discontinuity, including 'grain' boundaries between powder particles, generate intermediate shades of grey.
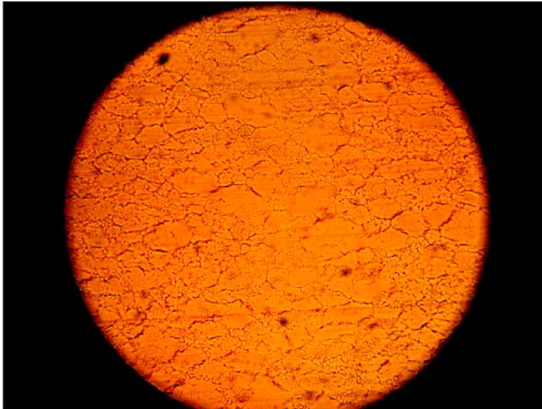
Fig. 7: Microtomed section from untested PE9 moulding, viewed in non-polarized transmitted light. Illuminated diameter of 0.8 mm. Buckley (OU).
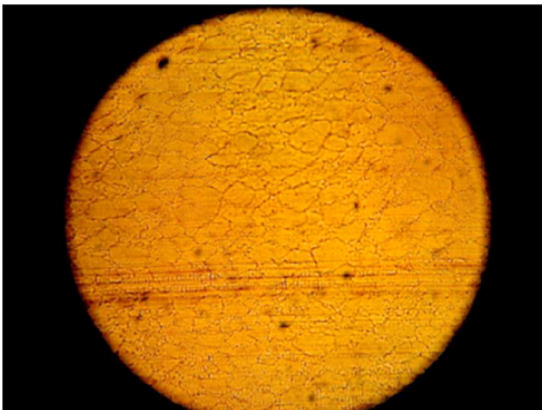

Fig. 8: Microtomed section from cyclically loaded PE5 moulding, viewed in non-polarized transmitted light. Loading direction horizontal. Illuminated diameter of 1.6 mm. Buckley (OU).

All three levels of scattering can be seen in Fig. 10. In particular, the granular structure of the mouldings is clearly defined, indicating that bonding between powder particles is less than ideal in the mouldings prepared by the polymer manufacturer for this project. That does not necessarily mean that they were too weak to make satisfactory orthopaedic implants. To determine the extent to which visible grain boundaries constitute active fusion defects, which could cause wear or fatigue problems in the more demanding prosthetic applications, it is necessary to measure resistance to mechanical failure and fracture, and to fatigue crack propagation in particular (see Part 4 in this series).

Conventionally, fusion defects are divided into two categories. Type 1 defects are defined as crack-like voids, where there is no contact between adjacent reactor powder particles. They are caused by inadequate compaction of the powder and are easy to detect. Type 2 defects are regions in which contact has been made during melt processing, but the quality of the bond is less than perfect; in these regions the polymer is not fully consolidated. This description covers a very broad range of imperfections, ranging from extremely weak regions, where little reptation has taken place across grain boundaries, to moderately strong bonds that are quite well established but have not reached the optimum level of entanglement density. Because reptation rates are low in UHMWPE, it is extremely difficult (and probably impossible) to achieve perfect bonding, where all traces of inter-particle boundaries have been eliminated and entanglement levels are comparable with those found, for example, in cast PMMA.
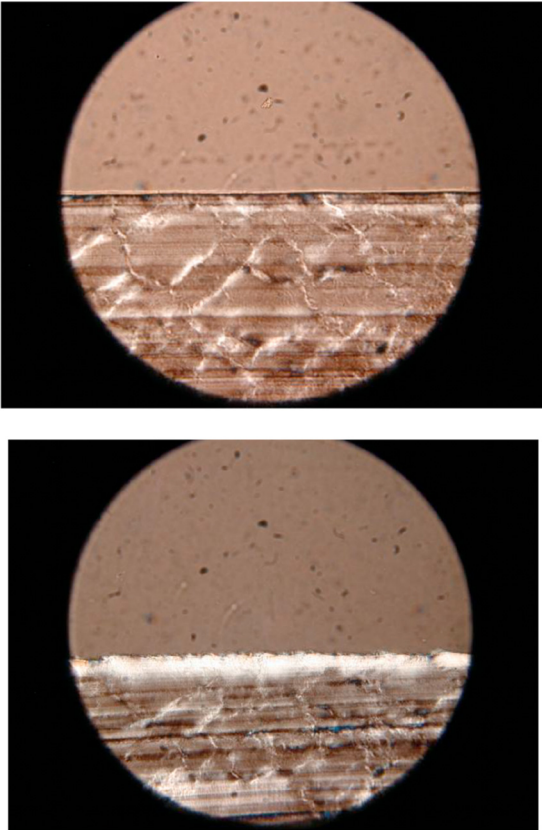
Fig. 9: Microtomed sections from PE5 tensile specimen, cut at 90 ° to the outer surface and viewed under polarized light. Top: untested specimen. Bottom: cyclically-loaded specimen, showing roughened surface. Tensile direction horizontal. Illuminated diameter 0.3 mm. Buckley (OU).
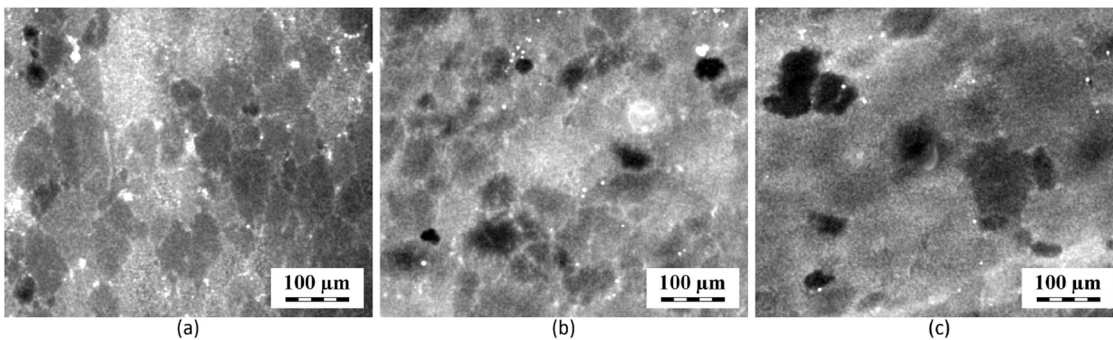

Fig. 10: Sections microtomed from UHMWPE mouldings, viewed in a light microscope using dark-field imaging: (a) PE06; (b) PE5; (c) PE9. Section thickness about 10 µm. Slouf (CZ).

3 Discussion

There are obvious problems in developing quality assurance procedures for UHMWPE, the most basic of which are discussed in Part 1. At the time of writing, it is impossible to measure molecular weight distributions – a key element in QA procedures for thermoplastics. The best available alternatives are to use intrinsic viscosity tests, and simply measure $\overline{M}_v$, or to estimate $\overline{M}_w$ using tensile creep tests at 150 °C, a few degrees above the melting point of HDPE. The accuracy of these creep measurements is questionable, because they are affected by

relatively low levels of entanglement at grain boundaries, where relaxation rates are high. This enhanced contribution to tensile drawing causes investigators to underestimate the true magnitude of $\overline{M}_\text{w}$. For quality assurance purposes, all of the methods currently used to characterize the molecular weight of UHMWPE are quite inadequate in comparison to size exclusion chromatography.

Apart from molecular weight distribution, the most significant factors affecting the performance of UHMWPE products are crystallinity, crystal structure, and entanglement. Characterizing crystallinity is straightforward; the scope and accuracy of measurements are not affected by high molecular weights. In the present project, standard DSC measurements showed that all of the freshly-made reactor powders had crystallinities above 70 %, and that PE06 powder was over 75 % crystalline – see Table 4.

Subsequent compression moulding led to a reduction in crystallinity in all three polymers, as shown in Section 2.4, Table 1 and Table 2. The crystallinity values obtained from IR spectroscopy are substantially higher than those determined using WAXS and DSC, but all three test methods showed that crystallinity was approximately 15 % higher in PE06 mouldings than in PE5 or PE9 mouldings. Although there is some scatter in the 1D⊥ column of Table 1 (for reasons that are unclear), the general trend is clear. Low chain mobility in the melt state placed restrictions on crystallization in PE5 and PE9. The (first peak) 2D SAXS data presented in Table 1 show that long periods in moulded UHMWPE increased steadily with increasing $\overline{M}_\text{w}$. Since most of the other test measurements covered in this report do not distinguish clearly between PE5 and PE9, there is perhaps a case for exploring the viability of 2D SAXS testing as a QA procedure.

From Tables 3 and 4 it is clear that annealing at high temperatures and pressures had a remarkable effect on melting point and crystallinity, especially in PE06, where χ_c approached 90 % in some samples and measured values of θ_m were close to (and in some cases higher than) the theoretical maximum melting temperature θ_m^0, which is 145.1 °C.

Similar but more extensive experiments were carried out in an earlier study by Yamazaki et al. on a fractionated linear polyethylene with $\overline{M}_\text{w}$ = 32 000 [12]. The samples were annealed in the hexagonal region of the phase diagram, where high chain mobility enabled the system to produce essentially defect-free chain-extended crystals. In this process, all entanglements were eliminated. On cooling under pressure (PT return route in Fig. 6), the crystals transformed from hexagonal to orthorhombic, but the chain-extended state was retained, free from entanglements. Subsequently, the samples were heated to 160 °C, conditioned for 5 min to produce an entangled melt, and crystallized isothermally at various temperatures, forming chain-folded lamellae. These experiments show that linear polyethylene is capable of forming ideal, defect-free crystals when the chains are very mobile. High temperatures and relatively low molecular weights enable them to approach this ideal state.

By contrast, annealing PE06, PE5, and PE9 for 1 or 2 h at 245 °C produced an increase in crystallinity, accompanied by some extension and alignment of the chains and loss of entanglements, but was unable to produce completely defect-free crystals. Instead, the long chains provided connections between crystalline blocks, which were separated by 'amorphous' regions in which the surviving entanglements were concentrated. The effect of annealing at 245 °C was to reduce N_e, the number of entanglements per unit volume, in each material, while increasing N_e locally in the inter-crystalline regions, because they occupied a reduced fraction of the total volume.

Studies by Bartczak [20], on a ram-extruded UHMWPE with a $\overline{M}_\text{w}$ of 0.6×10^6, showed that N_e fell from 5.7×10^{-26} m^{-3} in the extrudate to 2.6×10^{-26} m^{-3} in samples that were annealed in the hexagonal region and quenched under pressure to room temperature. Subsequent annealing of the melt at 160 °C resulted in an increase of N_e to 6.2×10^{-26} m^{-3}. During these experiments, crystallinity increased from 55.8 % initially to between 76 and 79 % in extended-chain samples, and fell to 44.6 % after annealing at 160 °C and recrystallizing.

Crystallinity has a strong influence on the mechanical properties of UHMWPE, which will be discussed in more detail in Part 3. However, it is not the only structural factor affecting performance. Uniaxial compression tests on HDPE over a range of strain rates have shown that yield stress increases with lamellar thickness, from 15 to 20 MPa when $L^\star$ is 20 nm to between 30 and 35 MPa when $L^\star$ reaches 40 nm. Beyond that point, further

increases in thickness have little effect [14]. In tension, cavitation of the soft 'amorphous' phase also plays an important part in yielding. Beyond the yield point, entanglement density plays a major part in controlling deformation behaviour, in particular the rate of strain hardening.

The results presented in this report provide some insight into the challenges encountered by manufacturers of UHMWPE components, especially those used in total joint prostheses. Ideally, the bonding between powder particles would be perfect. However, thermal degradation imposes upper limits on the temperatures and times involved in moulding or extrusion, and the long relaxation times of UHMWPE restrict the amount of reptation taking place during processing. Consequently, it appears to be impossible to eliminate fusion defects completely. Despite best efforts to optimize melt processing procedures, traces of the original powder-particle grain boundaries are always present in both moulded and extruded UHMWPE parts.

The presence of minor imperfections is not necessarily a serious problem in practical applications. From a QA perspective, the key question is not whether a particular moulding is defect-free, but whether it contains any imperfections that could significantly impair the performance of the moulding in service. Issues of this type arise in every branch of mechanical engineering. All load-bearing structures contain micro-cracks and other defects. The task of materials scientists and designers is to ensure that they do not lead to mechanical failure.

An essential element in the design procedure for load-bearing structures is reliable information about the maximum dimensions of potential crack initiation sites. That information is relatively easy to obtain in the case of metallic structures, but the same cannot be said of UHMWPE components. Fusion defects vary in severity from visible crack-like fissures to poorly defined regions with below-average entanglement densities. Current practice is simply to distinguish between open-void Type 1 defects, which cannot support tensile stresses, and void-free Type 2 defects, which have some load-bearing capacity, but are not as strong as the defect-free material. That classification is not particularly helpful. The practical challenge is to find a method for detecting and characterizing all fusion defects that have the capacity to diminish the performance of components in service, however difficult it is to identify them. A possible solution is proposed in Part 4 in this series, which describes the effectiveness of fatigue crack propagation testing in detecting weak bonding between powder particles in thick UHMWPE compact tension specimens.

4 Conclusions

This report assesses the strengths and limitations of current methods for characterizing supra-molecular structure in UHMWPE. By contrast to the problems encountered in obtaining reliable data on molecular weight distributions, accurate information about crystal structure, orientation, levels of degradation, and other structural features can be obtained without difficulty. Crystallinities determined using IR spectroscopy are higher than those measured using WAXS and DSC, but the discrepancy appears to be due to differences in the methods used for interpreting the data, rather than specific problems caused by ultra-high molecular weights. With increasing $\overline{M}_w$, SAXS patterns show a systematic increase in long period (from 31 to 39 nm to 45 nm) for reasons that have yet to be explained. Lamellar thicknesses are much lower than long periods, at between 9 and 12 nm – see Section 2.4. Crystallinity levels are between 70 and 80 % in powder obtained directly from the polymerization reactor, but decrease when the polymers are compression moulded, especially in PE5 and PE9, the two UHMWPE grades, where reduced relaxation rates in the melt hinder crystallization during cooling. Annealing at high temperatures and pressures, in the hexagonal region of the phase diagram, causes an increase in crystallinity and a reduction in the number of entanglements. Because long relaxation times generally enable some entanglements to survive this annealing procedure, entanglement densities are high in the inter-crystalline layers, especially in PE06.

The main structural problem affecting moulded and extruded UHMWPE is that interfaces between powder particles can fall below optimum strength, because of restricted reptation across grain boundaries. Raising the processing temperature above about 245 °C is not a viable option, because dwell temperatures and times are limited by thermal degradation. In light of these limitations, there is a need to develop more reliable methods

for characterizing fusion defects. Transmission optical microscopy of thin sections is capable of detecting some defects, which become more visible when a microtome blade cuts a thin section, thereby imposing large local stresses and strains on the material. There is scope for developing this approach further by using alternative methods for pre-conditioning specimens, in order to convert Type 2 fusion defects into micro-cracks. This approach will be considered in more detail in Part 3 of the series.

Membership of sponsoring body

Membership of the Subcommittee on Structure and Properties of Commercial Polymers during the preparation of these Reports was: Chair: Yongfen Men (China); **Secretary:** Yujing Tang (China); **Members:** Volker Altstädt (Germany); Lijia Am (China); Oliver Arnolds (USA); Dietmar W. Auhl (Netherlands); Paul Buckley (UK); Clive B. Bucknall (UK); Peng Chen (China); Ildoo Chung (S. Korea); Dirk J. Dijkstra (Germany); Andrzej Galeski (Poland); Christoph Gögelein (Germany); Chang-Sik Ha (S. Korea); Mijeong Han (S. Korea); Ulrich Handge (Germany); Jiasong He (China); Sven Henning (Germany); Jun-ichi Horinaka (Japan); Wenbing Hu (China); Dae Woo Ihm (S. Korea); Tadashi Inoue (Japan); Takaharu Isaki (Japan); Akihiro Izuka (Japan); Xiangling Ji (China); Michail Kalloudis (UK); Dukjoon Kim (S. Korea); Jin Kon Kim (S. Korea); Sung Chul Kim (S. Korea); Seong Hun Kim (S. Korea); D. Su. Lee (S. Korea); Won-Ki Lee (S. Korea); Jae Heung Lee (S. Korea); Soonho Lim (S. Korea); Chengyang Liu (China); Shu-ichi Maeda (Japan); Mario Malinconico (Italy); Goerg Michler (Germany); Koh-Hei Nitta (Japan); Ewa Piorkowska-Galeska (Poland); Jinliang Qiao (China); Artur Rozanski (Poland); Dong Gi Seong (S. Korea); Tongfei Shi (China); Hongwei Shi (China); Sampat Singh Bhatti (Germany); Miroslav Slouf (Czech Republic); Zhaohui Su (China); Toshikazu Takigawa (Japan); Katsuhisa Tokumitsu (Japan); Kenji Urayama (Japan); Tatana Vackova (Czech Republic); Silvie Vervoort (Netherlands); Iakovos Vittorias (Germany); Yanwei Wang (Kazakhstan); Jun Jie Wu (UK); Donghua Xu (China); Masayuki Yamaguchi (Japan); Myung Han Yoon (S. Korea); Wentao Zhai (China); Wim Zoetelief (Netherlands)

Membership of the IUPAC Polymer Division Committee for the period 2020–2021 is as follows: **President:** C. K. Luscombe (USA); **Past President:** G. T. Russell (New Zealand); **Vice President:** I. Lacík (Slovakia); **Secretary:** P. D. Topham (UK); **Titular Members:** M. C. H. Chan (Malaysia); C. Fellows (Australia); R. C. Hiorns (France); R. Hutchinson (Canada); D. S. Lee (Korea); John B. Matson (USA); **Associate Members:** S. Beuermann (Germany); G. Moad (Australia); Marloes Peeters (UK); C. dos Santos (Brazil); P. Théato (Germany); M. G. Walter (USA); **National Representatives:** Ana Aguiar-Ricardo (Portugal); Jiasong He (China); C.-S. Hsu (Taiwan); Melina T. Kalagasidis Krušić (Serbia); P. Mallon (South Africa); O. Philippova (Russia); Guido Raos (Italy); M. Sawamoto (Japan); A. Sturcova (Czech Republic); Jan van Hest (Netherlands).

References

[1] C. Bucknall, V. Altstädt, D. Auhl, P. Buckley, D. Dijkstra, A. Galeski, C. Gögelein, U. A. Handge, J. He, C. Y. Liu, G. Michler, E. Piorkowska, M. Slouf, I. Vittorias, J. J. W. *Pure Appl. Chem.* **92**, 1469 (2020).
[2] S. M. Kurtz. *UHMWPE Biomaterials Handbook*, Elsevier Amsterdam, 3rd ed. Amsterdam. (2015).
[3] D. Romano, E. Andablo-Reyes, S. Ronca, S. Rastogi. *Polymer* **74**, 76 (2015).
[4] A. Munoz-Eskalona, C. Villamizar, R. Frias. *Polym. Sci. Tech.* **22**, 95 (1983).
[5] H. D. Chanzy, J. F. Revol, R. H. Marchessault, A. Lamande, Z. Kolloid. *Z. Polym.* **25**, 563 (1973).
[6] G. H. Michler. *Kunststoff-Mikromechanik*, Carl Hanser Verlag, Munich (1992).

 [7] M. Slouf, H. Synkova, J. Baldrian, A. Marek, J. Kovarova, P. Schmidt, H. Dorschner, M. Stephan, U. Gohs. *J. Biomed. Res. B* **85**, 240 (2008).
 [8] M. Slouf, T. Vacklova, M. Nevora. *Polym. Testing* **41**, 191 (2015).
 [9] B. Wunderlich, G. Czornyi. *Macromolecules* **10**, 906 (1977).
[10] J. D. Hoffman, R. L. Miller. *Polymer* **38**, 3151 (1997).
[11] M. Hikosaka, K. Tsukijima, S. Rastogi. *A Keller. Polym.* **33**, 2502 (1992).
[12] S. Yamazaki, M. Hikosaka, A. Toda, I. Wataoka, F. Gu. *Polymer* **43**, 6585 (2002).
[13] M. Hikosaka. *Polymer* **28**, 1257 (1987).
[14] M. Hikosaka. *Polymer* **31**, 458 (1990).
[15] M. Psarski, E. Piorkowska, A. Galeski. *Macromolecules* **33**, 916 (2000).
[16] R. Masirek, E. Piorkowska, A. Galeski, A. Hiltner, E. Baer. *Macromolecules* **41**, 8086 (2008).
[17] A. Pawlak. *A Galeski. Polym.* **51**, 5771 (2010).
[18] A. Lazzeri, C. B. Bucknall. *J. Mater. Sci.* **28**, 6799 (1993).
[19] A. Lazzeri. C. B. Bucknall. Polymer **36**, 2895 (1995).
[20] Z. Bartczak. *J. Polym. Sci. B Polym. Phys.* **48**, 276 (2010).